Dimensionality-Mediated Semimetal-Semiconductor Transition in Ultrathin $PtTe_2$ Films

Meng-Kai Lin,[1,2] Rovi Angelo B. Villaos,[3] Joseph A. Hlevyack,[1,2] Peng Chen,[1,2,4,5] Ro-Ya Liu,[1,2,4,6] Chia-Hsiu Hsu,[3] José Avila,[7] Sung-Kwan Mo,[4] Feng-Chuan Chuang,[3,*] and T.-C. Chiang[1,2,†]

[1]*Department of Physics, University of Illinois at Urbana-Champaign, Urbana, Illinois 61801, USA*
[2]*Frederick Seitz Materials Research Laboratory, University of Illinois at Urbana-Champaign, Urbana, Illinois 61801, USA*
[3]*Department of Physics, National Sun Yat-Sen University, Kaohsiung 804, Taiwan*
[4]*Advanced Light Source, Lawrence Berkeley National Laboratory, Berkeley, California 94720, USA*
[5]*Shanghai Center for Complex Physics, School of Physics and Astronomy, Shanghai Jiao Tong University, Shanghai 200240, China*
[6]*Institute of Physics, Academia Sinica, Taipei 10617, Taiwan*
[7]*Synchrotron SOLEIL and Universite Paris-Saclay, L'Orme des Merisiers, BP48, 91190 Saint-Aubin, France*

(Received 5 September 2019; published 24 January 2020)

Platinum ditelluride ($PtTe_2$), a type-II Dirac semimetal, remains semimetallic in ultrathin films down to just two triatomic layers (TLs) with a negative gap of −0.36 eV. Further reduction of the film thickness to a single TL induces a Lifshitz electronic transition to a semiconductor with a large positive gap of +0.79 eV. This transition is evidenced by experimental band structure mapping of films prepared by layer-resolved molecular beam epitaxy, and by comparing the data to first-principles calculations using a hybrid functional. The results demonstrate a novel electronic transition at the two-dimensional limit through film thickness control.

DOI: 10.1103/PhysRevLett.124.036402

Transition metal dichalcogenides (TMDCs) form a vast family of van der Waals bonded quasi-two-dimensional materials. Their electronic properties span a broad spectrum including metals, semiconductors, and superconductors [1–8]. These properties tend to be largely unaffected as the materials are thinned down to just a few layers, but certain changes have been noted. As an example, bulk MoS_2, $MoSe_2$, and WSe_2 are indirect gap semiconductors, but the gaps become direct when the materials are thinned down to a single layer [5–8]. Such dimensional effects are of basic interest and can be utilized for property tuning. For the Pt-based TMDCs, the thickness dependence of the electronic structure is particularly strong based on recent calculations [9]. A number of experimental studies of ultrathin $PtSe_2$ and $PtTe_2$ have been carried out [10–14]. Both materials are semimetals in the bulk form, but they are expected to turn into a semiconductor in the single-layer limit. Wang *et al.* synthesized a single $PtSe_2$ TL on a Pt single crystal substrate through selenization of the Pt surface [10]. However, this method of growth has been limited to a single TL, which is furthermore electrically shorted out by the metallic substrate. Yan *et al.* utilized molecular beam epitaxy (MBE) to grow $PtSe_2$ films from 1 to 22 TL on graphene [14]. Their angle-resolved photoemission spectroscopy (ARPES) results reveal a semiconducting gap within this thickness range, although the bulk material should be a semimetal. By contrast, Deng *et al.* [15] reported that $PtTe_2$ films with thicknesses of 2 to 6 TL remain semimetallic with bands crossing the Fermi level; the predicted semiconducting phase at the single-TL limit has yet to be demonstrated. Our work, reported herein, on films of $PtTe_2$ of thicknesses 1 to 5 TL provides clear evidence that the semimetal-to-semiconductor transition does occur when the film thickness of $PtTe_2$ is reduced to a single TL. The gap for the single TL is quite large (0.79 eV based on theory), and thus the change in the electronic property represents an unusually strong Lifshitz transition. Detailed layer-resolved band mapping results are presented herein to illustrate the very large modifications in the electronic structure, including gap opening across the transition. The small electron pockets that appear at film thicknesses larger than 1 TL suggest that these $PtTe_2$ films are candidates for exhibiting an excitonic insulator phase [16–19].

Substrates of 6H-SiC(0001) were annealed repeatedly to form a well-ordered bilayer-graphene-terminated surface. $PtTe_2$ films were grown atop at a rate of 1 TL per hour by co-deposition of Pt and Te from an electron-beam evaporator and an effusion cell, respectively, with the substrate maintained at 280 C. After film growth, each sample was characterized by reflection high energy electron diffraction (RHEED) and by ARPES using a He lamp as the light source. Afterwards, each sample was capped with a 10 nm thick Te layer for protection. The capped samples, prepared in our home laboratory at the University of Illinois, were taken to beam line 10.0.1 at the Advanced Light Source (ALS) and the ANTARES beam line at the Synchrotron SOLEIL for detailed ARPES measurements. Each sample was decapped by heating to 300 C just prior to the ARPES measurements.

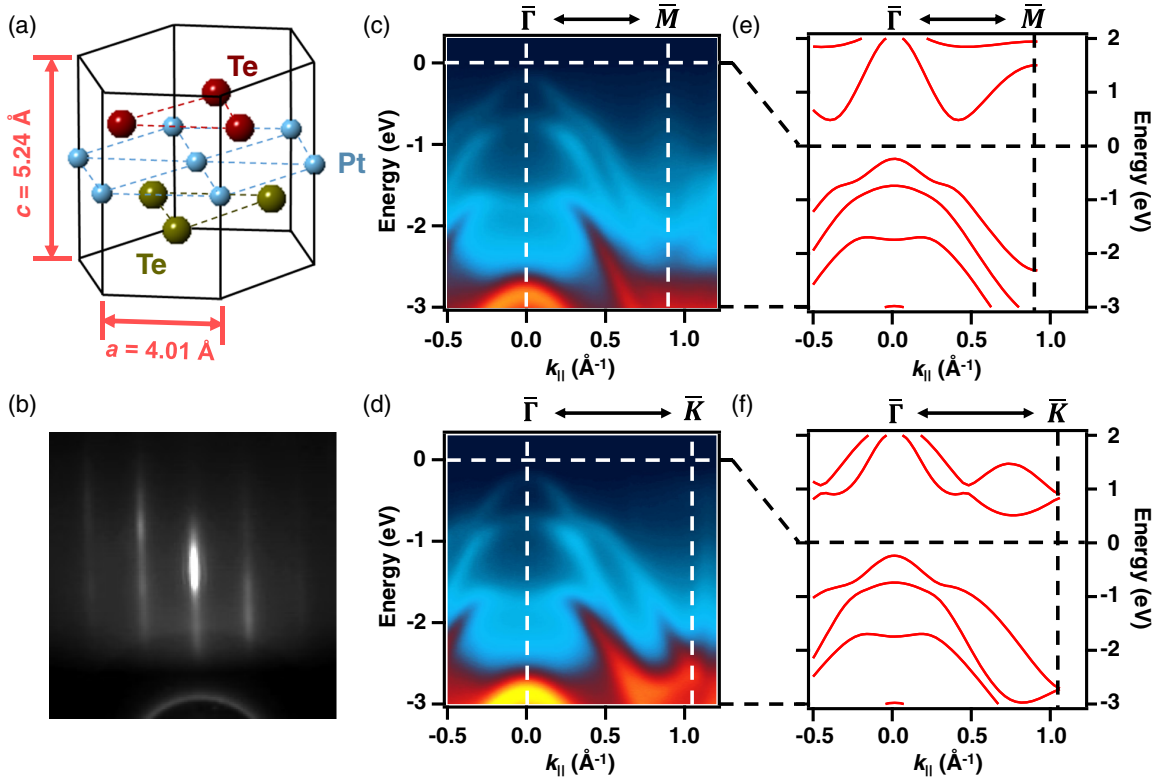

FIG. 1. Characterization of 1 TL $PtTe_2$. (a) Schematic atomic structure of $PtTe_2$. The lattice constants are indicated. (b) RHEED pattern taken from a 1 TL sample. (c) ARPES map along the $\overline{\Gamma M}$ direction taken with 53 eV photons from a 1 TL sample at 20 K. (d) Same as (c) but along the $\overline{\Gamma K}$ direction. (e) Calculated band structure along the $\overline{\Gamma M}$ direction. (f) Calculated band structure along the $\overline{\Gamma K}$ direction.

First-principles calculations were performed within the density functional theory framework [20] using both the Perdew-Burke-Ernzerhof (PBE) [21] functional and a hybrid functional (HSE06) [22] as implemented in the Vienna *ab initio* simulation package (VASP) [23]. The projector augmented wave (PAW) [24] pseudopotentials were chosen. The PBE functional and optB86b-vdW [25] van der Waals corrections were used for structure relaxation

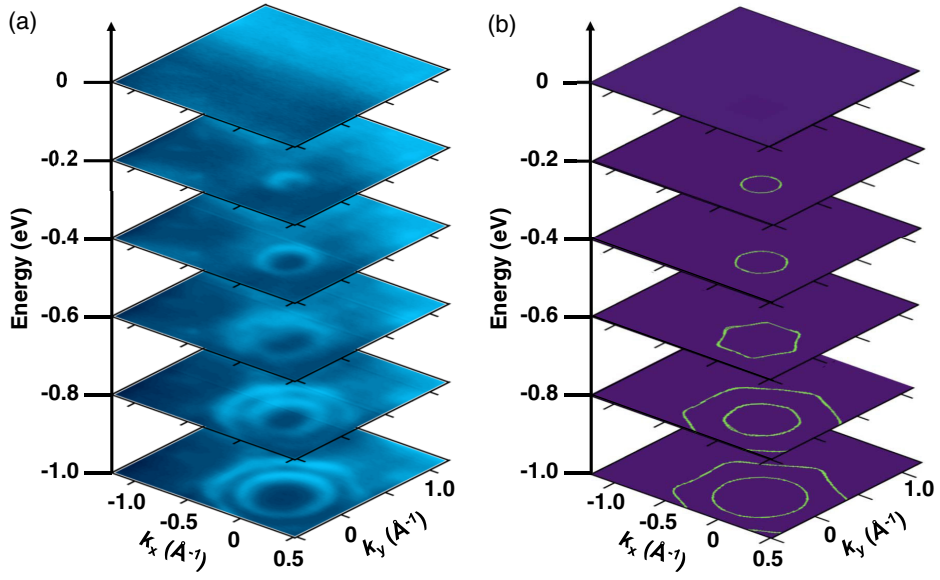

FIG. 2. ARPES maps revealing semiconducting nature of $PtTe_2$ 1 TL. (a) ARPES intensity maps at various energies for 1 TL $PtTe_2$ at 20 K taken with 53 eV photons. (b) Corresponding calculated constant-energy band contours.

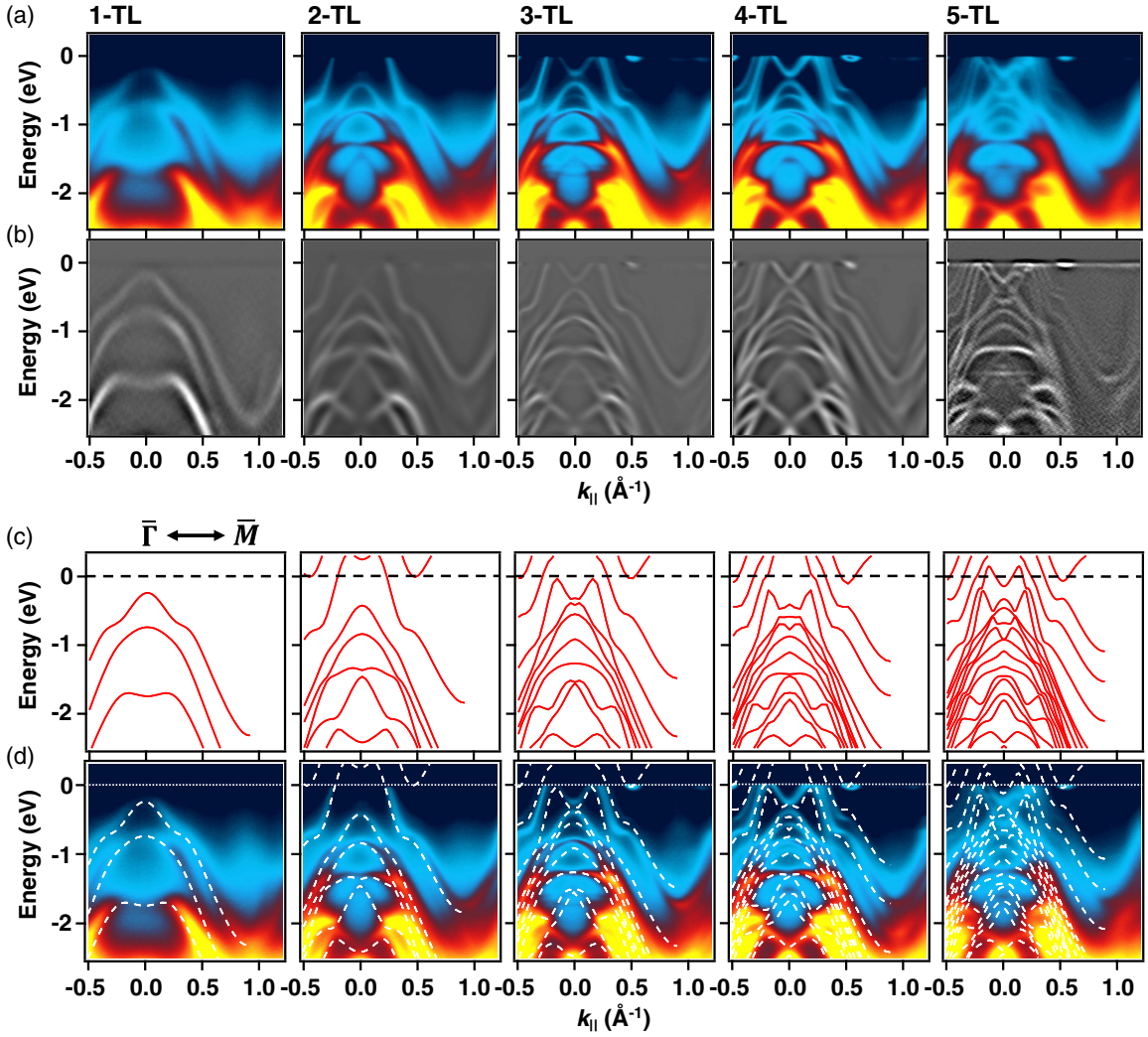

FIG. 3. Thickness dependent ARPES maps along the $\overline{\Gamma M}$ direction. (a) ARPES maps taken from 1, 2, 3, 4, and 5 TL samples at 20 K using 53 eV photons. (b) Corresponding maps of the second derivative of the ARPES intensity with respect to the in-plane momentum. (c) Corresponding calculated band structures. (d) ARPES data with the calculated band structure superimposed on top for a visual comparison.

with the residual forces set to less than 10^{-3} eV/Å. The self-consistent convergence criterion was set to 10^{-5} eV. Thin films were modeled by a periodic array separated by a vacuum gap of 20 Å. The first Brillouin zone was sampled using Γ-centered Monkhorst-Pack [26] grids of $24 \times 24 \times 1$ for the film structures. All band structures presented include spin-orbit coupling.

The atomic structure of a $PtTe_2$ TL is shown in Fig. 1(a), which consists of a triangular Pt atomic layer sandwiched in-between two triangular Te atomic layers. The bulk structure consists of a vertical stack of van der Waals bonded TLs separated by a relatively large lattice constant $c = 5.24$ Å. Thin films of $PtTe_2$ were grown by MBE on top of a bilayer-graphene-terminated 6H-SiC(0001) substrate [27–30]. *In situ* RHEED measurements reveal that the in-plane lattice constant of the films, $a = 4.01$ Å, is indistinguishable from the bulk value within our resolution, and the crystallographic orientation of the films is the same as that of the bilayer graphene substrate. The RHEED patterns are sharp, indicative of well-ordered films. An example of a RHEED pattern from a 1 TL film is shown in Fig. 1(b).

ARPES maps taken from a 1 TL sample along $\overline{\Gamma M}$ and $\overline{\Gamma K}$ [Figs. 1(c) and 1(d), respectively] show four valence bands within the energy range of 0 to −3 eV. These are in good agreement with corresponding results from first-principles density-functional calculations employing the Heyd-Scuseria-Ernzerhof (HSE) hybrid functional [Fig. 1(e) and Fig. 1(f), respectively]. The HSE functional is generally more accurate in predicting the band structure of semiconductors. The top three valence bands are dominated by the Te p orbitals as demonstrated in Fig. S1 in the Supplemental Material [31]. The fourth one at about −3 eV is mostly derived from the Pt d orbitals, which appears much more

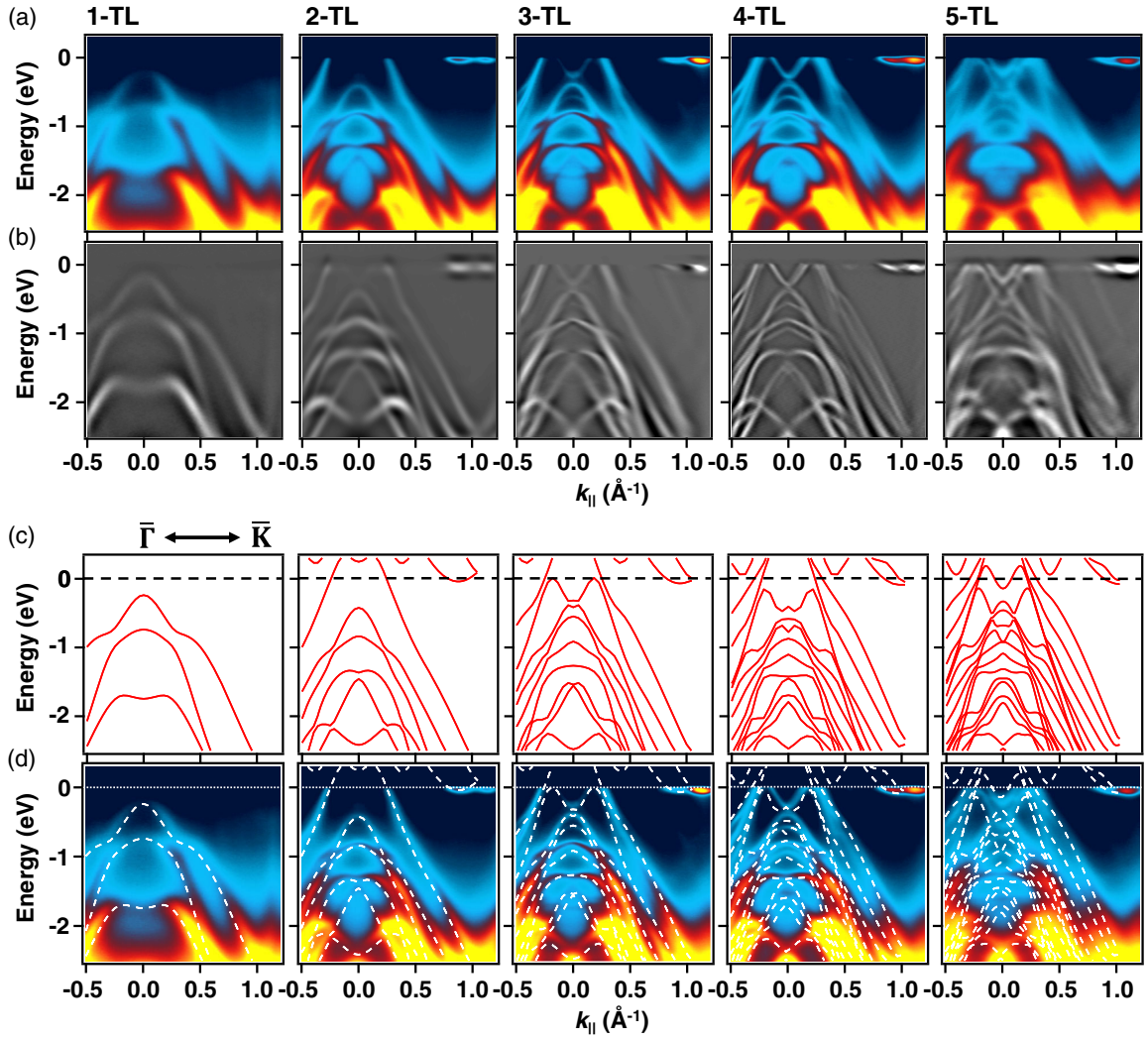

FIG. 4. Thickness dependent ARPES maps along the $\overline{\Gamma K}$ direction. (a) ARPES maps taken from 1, 2, 3, 4, and 5 TL samples at 20 K using 53 eV photons. (b) Corresponding maps of the second derivative of the ARPES intensity with respect to the in-plane momentum. (c) Corresponding calculated band structures. (d) ARPES data with the calculated band structure superimposed on top for a visual comparison.

intense in ARPES. Experimentally, the valence band maximum (VBM) is located at the zone center at an energy of −0.18 eV relative to the Fermi level. No conduction band features are observed in the experiment. The conduction band minimum (CBM) appears in between the $\bar{\Gamma}$ and $\bar{M}$ points, which yields an indirect gap of 0.79 eV according to theory [Fig. 1(e)]. Another local minimum in the conduction band occurs along the $\overline{\Gamma K}$ direction [Fig. 1(f)]. Our results establish that 1 TL $PtTe_2$ is a semiconductor with a sizable gap, which is quite different from the semimetallic electronic structure for multilayers and the bulk [9,15].

Figure 2(a) shows representative constant-energy ARPES cuts from the Fermi level down to −1 eV for the 1 TL sample. No structures are seen at the Fermi level. With decreasing energy, the cuts show a single point at the VBM, then a circle that expands, and then two distorted or warped concentric circles when the energy cuts through the two top valence bands. The contours show sixfold symmetry, confirming single-domain growth of the film. Theoretical energy contours of the bands [Fig. 2(b)] are in good agreement with the experiment. The indirect band gap as predicted by theory makes the system a good candidate for valleytronics. The situation is similar to that predicted for single-layer $PtSe_2$ and other related systems [11]. The good agreement between theory and experiment for the valence band dispersions in the present case gives confidence to this prediction.

ARPES maps for $PtTe_2$ films with thicknesses $N =$ 1–5 TL along the $\overline{\Gamma M}$ direction are presented in Fig. 3(a); maps for the second derivative of the ARPES intensity with respect to the in-plane momentum are presented in Fig. 3(b). Corresponding HSE bands, and the same bands with the ARPES data superimposed are shown in Fig. 3(c) and Fig. 3(d), respectively, for comparison. Similar results

for the $\overline{\Gamma K}$ direction are presented in Fig. 4. Evidently, strongly dispersing bands cross the Fermi level already at 2 TL, which marks a semiconductor-to-semimetal transition. This transition is characterized by an upward shift of the top valence band and a downward shift of the bottom conduction band for the single layer, and both bands cut through the Fermi level at 2 TL, resulting in a negative semimetallic gap of 0.36 eV. Cuts of the bands through the Fermi level, including tiny electron pockets, are best revealed by detailed Fermi surface mapping. The experimental results for the 1–5 TL films and corresponding theoretical calculations, shown in Fig. S2 in the Supplemental Material [31], are in good agreement.

The layer-by-layer band structure evolution in Figs. 3 and 4 follows a trend that each band for the single layer splits or multiplies into N bands for the N TL film. This band multiplication trend has been seen in numerous systems including simple metal films [34]. Specifically, there is just one valence band cutting through the Fermi level at 2 TL (Fig. 3), below which are 5 fully occupied valence bands with shapes in good agreement with theory. At 3 TL, two valence bands cut through the Fermi level, and the one closer to the zone center shows an M-like shape. Additional fully occupied valence bands emerge, and their shapes are again in good agreement with theory. Upon adding another TL to form a 4 TL film, the M-shaped valence band moves up slightly, and the band just below it splits around the zone center. The detailed band shapes are somewhat different from the theoretical results, but this level of minor discrepancy is not unusual for first-principles calculations. The band structure becomes very dense and seemingly complex at 5 TL. Still, the electronic structure is not at the bulk limit, where the system should become a type-II Dirac semimetal with a three-dimensional Dirac feature [9,13]. The question of two vs three dimensionality can be more accurately assessed by scanning the photon energy to map the k_z dependence. The results (Fig. S4 in the Supplemental Material [31]) confirm that the electronic structure at 5 TL is still two dimensional, but there is a hint of incipient three-dimensional behavior.

The large band splitting for increasing N in $PtTe_2$ is unusual for TMDCs, which tend to be quasi-two-dimensional. The band splitting is responsible for, in the present case, the semiconductor-to-semimetal transition between $N = 1$ and 2 and the strong band evolution at higher N. The underlying interaction is inter-TL coupling. The top valence bands near the Fermi level are dominated by the Te $5p$ orbitals. These orbitals from neighboring Te-Pt-Te layers do overlap somewhat across the van der Waals gap, which gives rise to a substantial bandwidth along the layer stacking direction. The same interaction gives rise to the three-dimensional Dirac cone in the bulk limit.

In conclusion, our study demonstrates a semimetal-to-semiconductor transition in $PtTe_2$ films when the film thickness is reduced to just a single layer. The band gap changes drastically from −0.36 at 2 TL to +0.79 eV at 1 TL according to theory. The resulting substantial positive gap for the single layer is unusual, and the indirect-gap band structure can be utilized for valleytronics applications. First-principles calculations show that the large changes of the electronic structure as a function of film thickness can be attributed to a significant interlayer coupling of the Te $5p$ orbitals across the van der Waals gaps between layers. Our findings establish a novel film-thickness-mediated Lifshitz electronic transition at the two-dimensional, single-layer limit.

This work is supported by the U.S. Department of Energy (DOE), Office of Science (OS), Office of Basic Energy Sciences, Division of Materials Science and Engineering, under Grant No. DE-FG02-07ER46383 (T. C. C.). F. C. C. acknowledges support from the National Center for Theoretical Sciences and the Ministry of Science and Technology of Taiwan under Grants No. MOST 107-2628-M-110-001-MY3. He is also grateful to the National Center for High-Performance Computing for computer time and support. This research used resources of the Advanced Light Source, which is a DOE Office of Science User Facility under Contract No. DE-AC02-05CH11231. The Synchrotron SOLEIL is supported by the Centre National de la Recherche Scientifique (CNRS) and the Commissariat à l'Energie Atomique et aux Energies Alternatives (CEA), France. This work was also supported by a public grant by the French National Research Agency (ANR) as part of the "Investissements d'Avenir" (reference: ANR-17-CE09-0016-05).

*Corresponding author.
fchuang@mail.nsysu.edu.tw
†Corresponding author.
tcchiang@illinois.edu

[1] B. Sipos, A. F. Kusmartseva, A. Akrap, H. Berger, L. Forró, and E. Tutiš, Nat. Mater. **7**, 960 (2008).
[2] M. N. Ali, J. Xiong, S. Flynn, J. Tao, Q. D. Gibson, L. M. Schoop, T. Liang, N. Haldolaarachchige, M. Hirschberger, N. P. Ong, and R. J. Cava, Nature (London) **514**, 205 (2014).
[3] Z. Wang, D. Gresch, A. A. Soluyanov, W. Xie, S. Kushwaha, X. Dai, M. Troyer, R. J. Cava, and B. A. Bernevig, Phys. Rev. Lett. **117**, 056805 (2016).
[4] H. Wang *et al.*, Nat. Commun. **8**, 394 (2017).
[5] R. Roldán, J. A. Silva-Guillén, M. P. López-Sancho, F. Guinea, E. Cappelluti, and P. Ordejón, Ann. Phys. (Berlin) **526**, 347 (2014).
[6] W. Zhao, Z. Ghorannevis, L. Chu, M. Toh, C. Kloc, P. H. Tan, and G. Eda, ACS Nano **7**, 791 (2013).
[7] K. F. Mak, C. Lee, J. Hone, J. Shan, and T. F. Heinz, Phys. Rev. Lett. **105**, 136805 (2010).
[8] A. Splendiani, L. Sun, Y. Zhang, T. Li, J. Kim, C. Y. Chim, G. Galli, and F. Wang, Nano Lett. **10**, 1271 (2010).

[9] R. A. B. Villaos, C. P. Crisostomo, Z. Q. Huang, S. M. Huang, A. A. B. Padama, M. A. Albao, H. Lin, and F. C. Chuang, NPJ 2D Mater. Appl. **3**, 2 (2019).
[10] Y. Wang *et al.*, Nano Lett. **15**, 4013 (2015).
[11] W. Yao, E. Wang, H. Huang, K. Deng, M. Yan, K. Zhang, K. Miyamoto, T. Okuda, L. Li, Y. Wang, H. Gao, C. Liu, W. Duan, and S. Zhou, Nat. Commun. **8**, 14216 (2017).
[12] Y. Li, Y. Xia, S. A. Ekahana, N. Kumar, J. Jiang, L. Yang, C. Chen, C. Liu, B. Yan, C. Felser, G. Li, Z. Liu, and Y. Chen, Phys. Rev. Mater. **1**, 074202 (2017).
[13] M. Yan, H. Huang, K. Zhang, E. Wang, W. Yao, K. Deng, G. Wan, H. Zhang, M. Arita, H. Yang, Z. Sun, H. Yao, Y. Wu, S. Fan, W. Duan, and S. Zhou, Nat. Commun. **8**, 257 (2017).
[14] M. Yan, E. Wang, X. Zhou, G. Zhang, H. Zhang, K. Zhang, W. Yao, N. Lu, S. Yang, S. Wu, T. Yoshikawa, K. Miyamoto, T. Okuda, Y. Wu, P. Yu, W. Duan, and S. Zhou, 2D Mater. **4**, 045015 (2017).
[15] K. Deng, M. Yan, Z. Yu, J. Li, X. Zhou, K. Zhang, Y. Zhao, K. Miyamoto, T. Okuda, W. Duan, Y. Wu, X. Zhong, and S. Zhou, Sci. Bull. **64**, 1044 (2019).
[16] F. X. Bronold and H. Fehske, Phys. Rev. B **74**, 165107 (2006).
[17] K. Okazaki, Y. Ogawa, T. Suzuki, T. Yamamoto, T. Someya, S. Michimae, M. Watanabe, Y. Lu, M. Nohara, H. Takagi, N. Kayatama, H. Sawa, M. Fujisawa, T. Kanai, N. Ishii, J. Itatani, T. Mizokawa, and S. Shin, Nat. Commun. **9**, 4322 (2018).
[18] K. Fukutani, R. Stania, J. Jung, E. F. Schwier, K. Shimada, C. I. Kwon, J. S. Kim, and H. W. Yeom, Phys. Rev. Lett. **123**, 206401 (2019).
[19] Y. F. Lu, H. Kono, T. I. Larkin, A. W. Rost, T. Takayama, A. V. Boris, B. Keimer, and H. Takagi, Nat. Commun. **8**, 14408 (2017).
[20] P. Hohenberg and W. Kohn, Phys. Rev. **136**, B864 (1964).
[21] J. P. Perdew, K. Burke, and M. Ernzerhof, Phys. Rev. Lett. **77**, 3865 (1996).
[22] A. V. Krukau, O. A. Vydrov, A. F. Izmaylov, and G. E. Scuseria, J. Chem. Phys. **125**, 224106 (2006).
[23] G. Kresse and J. Hafner, Phys. Rev. B **47**, 558 (1993).
[24] P. E. Blöchl, Phys. Rev. B **50**, 17953 (1994).
[25] J. Klimeš, D. R. Bowler, and A. Michaelides, J. Phys. Condens. Matter **22**, 022201 (2010).
[26] H. J. Monkhorst and J. D. Pack, Phys. Rev. B **13**, 5188 (1976).
[27] P. Chen, Y.-H. Chan, M.-H. Wong, X.-Y. Fang, M. Y. Chou, S.-K. Mo, Z. Hussain, A.-V. Fedorov, and T.-C. Chiang, Nano Lett. **16**, 6331 (2016).
[28] P. Chen, W. W. Pai, Y.-H. Chan, A. Takayama, C.-Z. Xu, A. Karn, S. Hasegawa, M. Y. Chou, S.-K. Mo, A.-V. Fedorov, and T.-C. Chiang, Nat. Commun. **8**, 516 (2017).
[29] P. Chen, W. W. Pai, Y.-H. Chan, V. Madhavan, M. Y. Chou, S.-K. Mo, A.-V. Fedorov, and T.-C. Chiang, Phys. Rev. Lett. **121**, 196402 (2018).
[30] P. Chen, W. W. Pai, Y.-H. Chan, W.-L. Sun, C.-Z. Xu, D.-S. Lin, M. Y. Chou, A.-V. Fedorov, and T.-C. Chiang, Nat. Commun. **9**, 2003 (2018).
[31] See Supplemental Material at http://link.aps.org/supplemental/10.1103/PhysRevLett.124.036402 for detailed information about the comparison of PBE and HSE calculations and additional data from ARPES band mapping, which includes Refs. [32,33].
[32] D. Pierucci, H. Henck, J. Avila, A. Balan, C. H. Naylor, G. Patriarche, Y. J. Dappe, M. G. Silly, F. Sirotti, A. T. C. Johnson, M. C. Asensio, and A. Ouerghi, Nano Lett. **16**, 4054 (2016).
[33] A. Bostwick, T. Ohta, T. Seyller, K. Horn, and E. Rotenberg, Nat. Phys. **3**, 36 (2007).
[34] T. C. Chiang, Surf. Sci. Rep. **39**, 181 (2000).